Numerical modelling of CO_2 migration in heterogeneous sediments and leakage scenario for STEMM-CCS field experiments

Umer Saleem[a], Marius Dewar[a,b], Tariq Nawaz Chaudhary[a], Mehroz Sana[a], Anna Lichtschlag[d], Guttorm Alendal[c], Baixin Chen[a,*]

[a] *Institute of Mechanical, Process and Energy Engineering, Heriot-Watt University, Edinburgh, EH14 4AS, UK*

[b] *Plymouth Marine Laboratory, Prospect Place, Plymouth, PL1 3DH, UK*

[c] *Department of Mathematics, University of Bergen, Bergen, Norway*

[d] *National Oceanography Centre, Southampton, UK*

*: corresponding author, b.chen@hw.ac.uk

Abstract

The dynamics and plume development of injected CO_2 dispersion and dissolution through sediments into water column, at the STEMM-CCS field experiment conducted in Goldeneye, are simulated and predicted by a newly developed two-phase flow model based on Navier-Stokes-Darcy equations. In the experiment, CO_2 gas was released into shallow marine sediment 3.0 m below the seafloor at 120 m water depth in the North Sea.

The pre-experimental survey data of porosity, grain size distributions, and brine concentration are used to reconstruct the model sediments. The gas CO_2 is then injected into the sediments at a rate of 5.7 kg/day to 143 kg/day. The model is validated by diagnostic simulations to compare with field observation data of CO_2 eruption time, changes in pH in sediments, and the gas leakage rates. Then the dynamics of the CO_2 plume development in the sediments are investigated by model simulations, including the leakage pathways, the fluids interactions among CO_2/brine/sediments, and CO_2 dissolution, in order to comprehend the mechanisms of CO_2 leakage through sediments. It is shown from model simulations that the CO_2 plume develops horizontally in the sediments at a rate of 0.375 m/day, CO_2 dissolution in the sediments is at an overall average rate of 0.03g/sec with some peaks of 0.45g/sec, 0.15g/sec, and 0.3g/sec, respectively, following the increases in injection rates, when some fresh brine provided. These, therefore, lead to a ratio of 0.90~0.93 of CO_2 leakage rate to injection rate.

Keywords: STEMM-CCS, CO_2 injection, Two-Phase Flow in porous media, porosity and grain size distribution, Gas migration, Darcy Resistance, Carbon Capture and Storage, CO_2 Leakage, Pipe Flow, CO_2 Dissolution

1 Introduction

Carbon capture and storage (CCS) is a vital solution to mitigate the climate change and/or ocean acidification accompanying anthropogenic carbon dioxide (CO_2) level increasing by more than 25% since 1959 [1]. The carbon emission has resulted in global warming of 1.5 °C above pre-industrial levels and affected natural habitats on/off shore [2]. CCS offers a solution of the disposal of carbon dioxide (CO_2) in the overburden sub-seabed reservoirs/geological structures instead of emitting the gas into the atmosphere to meet the 'target' set by the Kyoto Protocol [3, 4].

The geological reservoirs can be chosen for long term storage of CO_2 in well-designed storage sites[5]. The utmost important concern about implementing CCS, especially for CO_2 under seabed reservoir storage, is the leakage risk of the sequestrated CO_2 to the ocean due to its environmental physicochemical impacts [6]. The impacts include the local acidification at the CO_2 leakage site [7, 8] and the effects on marine life and ecosystem [9-11]. Therefore, it is necessary to understand the leakage mechanisms, then to estimate or predict the potentials of the leakage to reduce the associated risks.

For under-seabed storage, studies have been made from Lab experiments [12, 13], the natural CO_2 migration through geoformations into the ocean, to the designed filed experiments, in collaboration with the studies of CO_2 ocean storage [14-17]. It has been recognized that CO_2 leakage developments are at a range of spatial scales from pore (~mm) in the geoformation, the bubble/droplet (~ cm) once leaked into ocean, then the regional (~ 10^2 km) to global in the ocean. Liquid and gas phase CO_2 plume developments in turbulent ocean has been observed from small scale field experiments [18, 19] and modeled by means of computational fluid dynamics (CFD) [14, 20] (Umer, add this paper to here, Sato, T.; Sato, K. Numerical prediction of the dilution process and its biological impactsonCO2 ocean sequestration. J. Marine Sci. Technol. 2002, 6, 169-180.) and a kind of integral plume models (Dissanayake et al., 2018). The data of changes in pH from these small-scale plume models had been successfully implemented, as the input parametric data for plume further movements, in the large-scale ocean models (Blackford et al, 2020) once CO_2 leaks from seabed. On the other hand, the CO_2 mitigation from storage reservoirs to sediments were widely investigated from the field observations [21], the Lab experimental studies [22, 23] and numerical simulations [24-27]. However, leakage from sediments into the ocean turbulent bottom boundary layers (TBBL) has been less focused, which, however, is one of the key processes for assessments of the biological impacts of leaked CO_2 on the ocean, as a rich population of marine organisms resides within both the ocean TBBL and shallow sediments. It is the dynamics of CO_2 migration and dissolution crossing the interface between shallow sediments and oceanic TBBL that dominate the leakage sources to the plumes evaluations in the ocean [15].

In order to ensure the effective environmental monitoring of offshore CCS storage sites, the Strategies for Environmental Monitoring of Marine Carbon Capture and Storage (STEMM-CCS) project was launched in 2016 [28], following previous field experiments QICS [29] and ECO2 [21]. STEMM-CCS is a scientific research project to simulate a sub-seafloor CO_2 leak under real-life conditions in the North Sea [28]. One of the primary objectives of the project is to produce experimental data for the development and calibration of numerical models to simulate the leakage dynamics of CO_2 out of the geoformations with the knowledge of dispersion time, pathways through faults and high permeable zones. In terms of marine physiochemical and biological impacts, for instance, the changes in pH due to leaked CO_2 is one of the most significant data for the assessment of leakage and model calibrations. Adequate knowledge of CO_2 dispersion through complex structure geoformation and dissolution characteristics of developed plume are mandatory and vital towards the development of the leakage

prediction models. Supported by the project, a so-called Arbitrary Navier-Stokes-Darcy multi-fluid flow model (AnsdMF) has been developed for simulations of CO_2 transportations through the sediments with complex structures into the turbulent ocean.

In this study, the AnsdMF model is applied to simulate and predict the dynamic processes of initiations and developments of CO_2 and CO_2 solution plumes from injection ports through sediments to the ocean current in STEMM-CCS experiment. The numerical model settings, including the data collections, analysis, and reconstruction of sediments, are discussed in Section 2. The overall methodology of numerical model including sub models of mass, momentum, and interfacial interactions among fluid-fluid-solid are explained in Section 3. The analysis and discussions on the model diagnostic simulation results are made in Section 4 with the CO_2 injection through pipe and leakage scenario results. Finally, the conclusions are drawn in Section 5.

2 Model Sediment Setup and Data Collection

The CO_2 release experiment of STEMM-CCS project was carried out in the vicinity of the Goldeneye platform located in a sandstone formation of Early Cretaceous near Scotland beneath Moray Firth (56-60˚N) [30]. In this project, gas CO_2 supplied from gas tanks was controllably released from 3m underneath the seabed[31]. Ships, remotely operated vehicles (ROVs) and autonomous underwater vehicles (AUVs), the gas sampling system, and related equipment and sensors were employed to measure the changes in physicochemical properties in seawater and brine and monitor the leakages of CO_2. The gas release started on 11/05/2019 at 15:19hrs, when is set as the start of day 0 of the experiment [32] in this study. The data of CO_2 injection rate and the total CO_2 injected, as shown in Fig. 1, are collected from field experiment as the input data of the modeling.

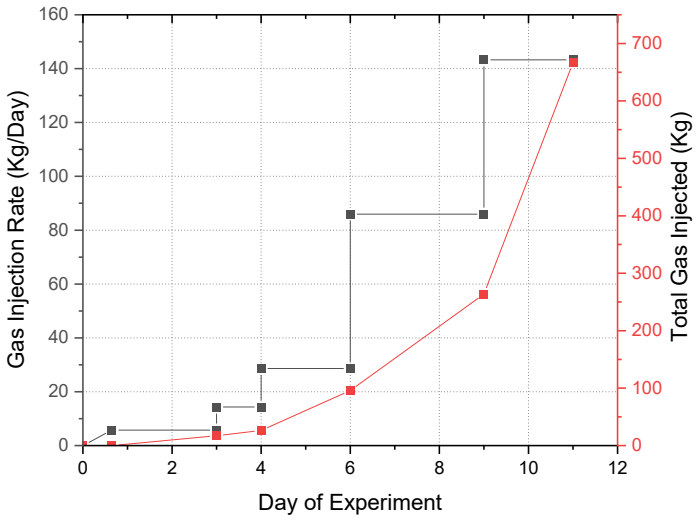

Figure 1: *Gas injection rate and total gas injected over the days from start injection collected from field experiment [32]*

2.1 Porosity and Grain Size Distribution

To set up the model sediments, AnsdMF requires data of particle size distributions and the porosity distributions of sediments. The data obtained from project pre-survey were collected, which are those sampled in 18 boxes at different locations around CO_2 injection site down to 5.0 meters. The porosity data from core samples used in this study are plotted in Fig 2, on which are the data from landers (POS527/si83 and gravity corer GC-06-Station-102), pockmarks (GC-01-Station-97 st.90/91 Obj 103), and well (GC-07-Station-103). The data shows that the average porosity is around 53% with +10% and –20% for the sediments deeper than 16 cm (Fig. 2 left), while, the good distributions from surface to the depth of 16cm for shallow sediments (Fig. 2 right).

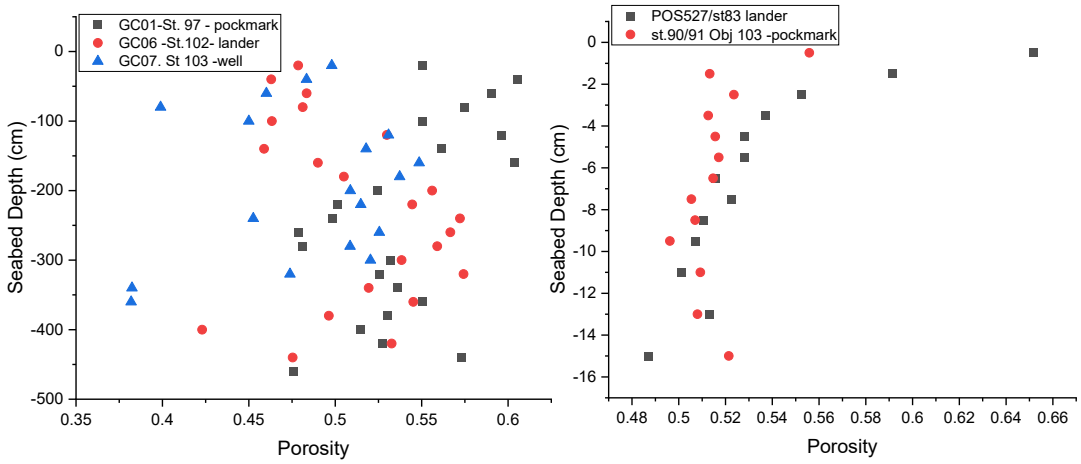

Figure 2: *Porosity distribution along the depth up to 500cm (left) and the shallow sediment (right)* from various locations [33].

Another set of data requested from setting the model is the particle size distributions, which are taken from Particle size analysis (PSA) for various samples collected at different depths of sediments [33]. A brief discussion on the characteristics of the particle distribution will help for model setting and for modelling the dynamic process of CO_2 gas penetration through sediments. From the data, shown in Fig. 3, it can be found that the deeper sediments, 3–4 m below the seabed (data of GC3 398-412cm), are mostly the fine sand of laminated mud. The surface sediments down to about 0.5m, however, most of the particles are of 60-100 μm with some smaller particles of smaller than 10 μm. On between of those layers is a layer of a mixture of substances with varied grain sizes dominated within 8 to 100 μm. It must be noted that the very small particles within the sediments are more sensitive to the additional disturbances, such as the penetration of CO_2 into the sediments, while the larger particles have a relatively larger inertia to 'against' the disturbances and keep their original positions. This behavior of particles can be utilized for diagnostic setting the model sediments for prediction of CO_2 dispersion with comparisons of observation data, such as the eruption time.

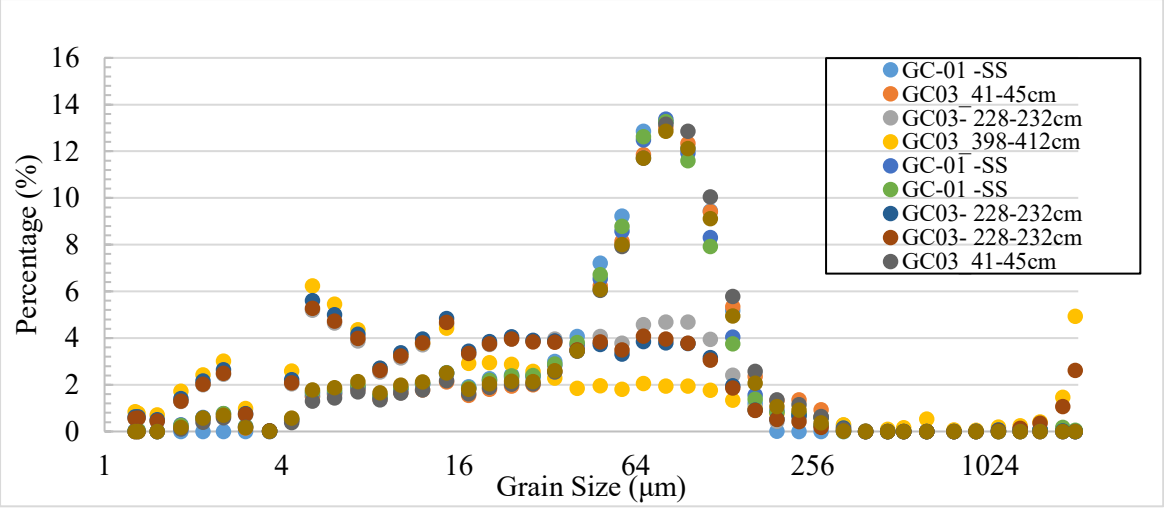

Figure 3: *Particle size density from various cores. GC01 to GC03 are the data from gravity cores followed by the depth in centimetre, while, the SS means the shallow sediments.*

2.2 Reconstruction of model sediments by data

The heterogenous sediments are sediments with complex structure and various pore throat size distributions. The model requires the permeability distribution, intrinsic permeability at the first stage, to predict the resistant forces of fluids and porous solids. For the heterogeneous sediment or rock, the throat size varies depending on the inter-connected pore structure and the pore size distribution, which is a function of porosity ε and particle size. Clay or poorly sorted silt shows lower permeability whereas coarse or well-sorted sediment, such as by shelly sands, shows high permeability [34]. The correlations of permeability are mostly developed from the data of experiments and highly dependent on the structures of sediments. In this study, the Kozeny-Carman's correlation [35] for intrinsic permeability is applied for reconstructions of shallow sands sediments,

$$\boldsymbol{K} = \frac{d_p^2}{180}\frac{\varepsilon^3}{(1-\varepsilon)^2} \tag{1}$$

where, K is intrinsic permeability (m^2) and d_p is the particles size (m). The data of porosity and particles size distributions from field observations as shown in Fig 2 & 3 are used to reconstruct the model sediments in term of intrinsic permeability using Eq (1) and the 'topoSet' utility tool available on OpenFOAM [36]. The data with a range of the variation of both the porosity and particle size at a given depth are randomly taken to set the distributions of intrinsic permeability horizontally, meanwhile, the interpolations are made to set the data for the meshes on between the data available layers. The intrinsic permeabilities averaged at selected layers from reconstructed sediments can be found from Fig. 4 (a) and the reconstructed sediment demonstrated by intrinsic permeabilities for the computational domain of 10mx5m (horizontal)x7m (vertical) for sediment is given in Fig. 4 (b). The permeability of the meshes between depth from 4.5m to 7.0 m (no data available) is set by randomly selecting the data at layer 4.5m. From such a reconstruction, it has been noticed that there are no specific structures, such

as called as ‘chimney’ or ‘fractures’ or even the ‘pockmarks’ could be generated, which were identified from field observations at the leakage sites. In this study, such a complex structure sediment is generated by performing diagnostic simulations. The details can be found from section 3.2.

The basic idea is from the general physics briefly described as follows. Fluids stored in the porosity of rocks produce pore pressure. Based on the magnitude, pore pressure can be normal/hydrostatic, sub-normal/sub-hydrostatic or abnormal/over pressured [37]. It depends on the sediments’ strength that the formation or structure can bear the particular pressure before failing and developing to the fractures. When the pore pressure exceeds the overburden pressure due to CO_2 injection or flowing into, small diameter particles (mad or clay) may flow away to produce channels or fractures. The model sediments are reconstructed in such a way to simulate the effect of chimney, fractures, and pockmarks by using the data from observations (Section 2.1) and setting the cut-off grain sides (the sides of the particles moveable) to create the chimney (or pipeline, fracture) in the sediments. The grain/particles smaller than the cut-off grain size are considered as the movable particles as CO_2 penetration in. As shown from numerical experiments (section 3.2), this cut-off grain size is diagnosed as 60 μm to represent the data of gas dispersion time of ~16 mins.

From the simulations of CO_2 dispersion and dissolution through the reconstructed sediments with grain size cut-off, it is also identified that the fine grains with size smaller than 60 μm could possibly be pushed up as like ‘clay’ to form the ‘pockmarks’ on the seafloor, providing the high permeability as observed from field survey. This means the gas could manage to create their own pathways, the chimney, or the fracture channel, or the pipelines, by driving the fine size grains up from original place in the sediment. This can be demonstrated by the CO_2 plumes at the dispersion time (the time reaching to the seafloor), as described in section 3.2.

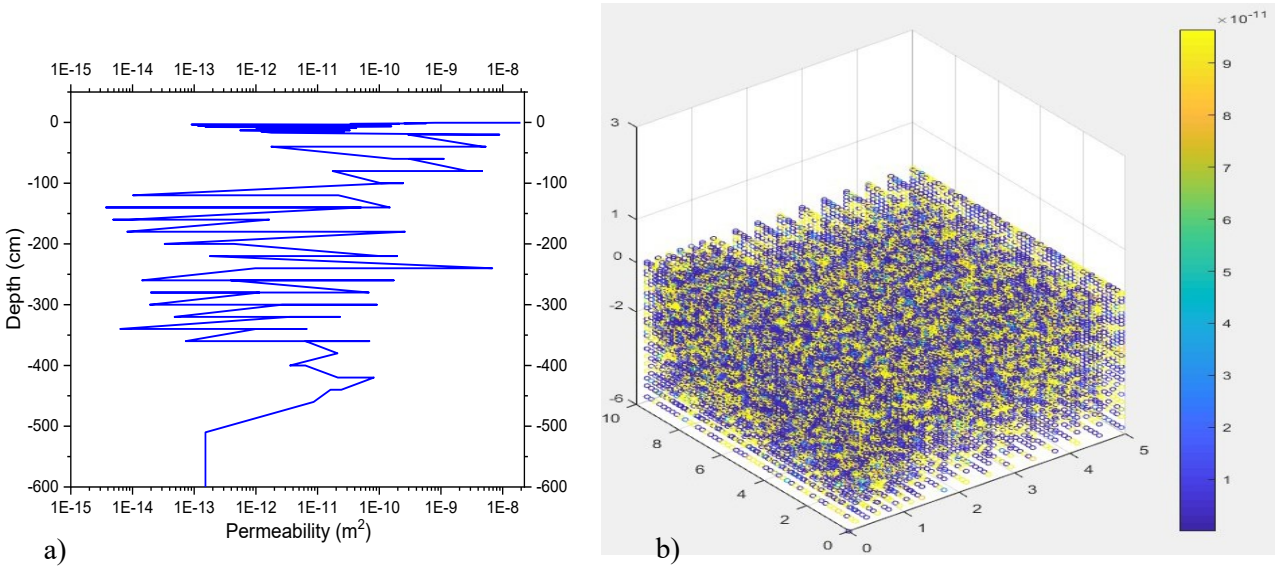

Figure 4: *(a) Horizontal Averaged Permeability distribution against depth calculated by Eq (1) using experimental data of particles size and porosity (shown in Fig. 2 and Fig 3) ;(b) permeability distribution in the computational domain reconstructed*

3 Simulation Model and Governing Equations

The dynamics of two-phase flows of leaked CO_2 flow through the sediments into the turbulent sea bottom boundary layers (BBL) are modeled by a set of Naiver-Stokes-Darcy equations under assumptions of fluids and sediment are in the thermal equilibrium state with no thermal impacts considered, e.g., the dissolution heat, within model considered scales of 10 to 20 meters in this study. The model simulates the mass and momentum exchanges of fluids/phases in Eulerian scheme and couples the turbulent ocean flows with the flows in sediments. Due to the dynamics coupling of ocean current, the fluids flow in the sediments can be generated by the flows of BBL. The momentum interactions between phases/fluids are modeled individually by implementing the correlations from either the experimental data or theoretical analysis into the governing equations as the source terms.

Considering the multiphase flows, the ensemble averaged continuity equations for phase φ can be written as

$$\frac{\partial \alpha_\varphi \varepsilon\, \rho_\varphi}{\partial t} + \frac{\partial}{\partial x_i}(\varepsilon \alpha_\varphi \rho_\varphi \overline{U}_{\varphi,i}) = \dot{S}_{m,\varphi} \tag{2}$$

where α_φ, ρ_φ and $\overline{U}_{\varphi,i}$ are the volume fraction, density, and the average velocity of phase φ. ε represents the porosity of sediments and $\dot{S}_{m,\varphi}$ is source term of the interphase mass transfer. Hence, in the BBL of ocean, $(\varepsilon \to 1)$, Eq (2) shrinks to a closing form of conditionally averaged continuity equation of phase φ as,

$$\frac{\partial \alpha_\varphi}{\partial t} + \nabla.\left(\alpha_\varphi . \overline{U}_{\varphi,i}\right) + \nabla.\left(\alpha_\varphi (1-\alpha_\varphi).\overline{U}_{r,i}\right) = \dot{S}_{\alpha,\varphi} \tag{3}$$

The last term on the left side of Eq (3) is the term for restoring immiscibility condition of the two fluids with $\overline{U}_{ri}$ the characteristic compression velocity of the interface sharpening can be predicted by the relative velocities between the fluids. Here in this paper, φ =1 and φ =0 represent the CO_2 and seawater, respectively.

Considering the interactions among phases/fluids and solid pore structure sediments, the ensemble averaged momentum equations for phase φ are given by:

$$\begin{aligned} &\frac{\partial \varepsilon \alpha_\varphi \rho_\varphi \overline{U}_{\varphi,i}}{\partial t} + \frac{\partial}{\partial x_j}\left(\varepsilon \alpha_\varphi \rho_\varphi \overline{U}_{\varphi,i}\overline{U}_{\varphi,j}\right) + \frac{\partial}{\partial x_j}\left(\varepsilon \alpha_\varphi \rho_\varphi \overline{R}_{\varphi,i}\right) \\ &= -\varepsilon \alpha_\varphi \nabla \bar{p}_\varphi + \nabla.(\varepsilon \alpha_\varphi \bar{\tau}_\varphi) + \varepsilon \alpha_\varphi \rho_\varphi g + F_{b,\varphi} + \varepsilon M_\varphi \\ &- M_{\varphi,s} \end{aligned} \tag{4}$$

where, $\bar{R}_{i,j}$ is the combined Reynolds turbulent stress, $\bar{p}$ the pressure, $\bar{M}_{\varphi}$ the averaged inter-fluid phase momentum transfer term, $F_{b,\varphi}$ the body force, and $\bar{M}_{\varphi,s}$ the total resistance source term from sediments derived using Darcy-Forchheimer's law, of which should be modelled for the simulations.

The inter-fluid phase momentum transfer includes the instantaneous drag, lift, virtual mass and Basset forces, of which only the drag force (F_d) is considered in this study as it dominates,

$$M_{\varphi} = \alpha_{\varphi} F_d / V \tag{5}$$

where V is the volume of the dispersed phase element (DPE) and,

$$F_d = \frac{1}{2}\rho_{\varphi} A C_d |\bar{U}_r| \bar{U}_r \tag{6}$$

where A is the projected area of dispersed phase that is normal to relative velocity $\bar{U}_r$ and C_d is drag coefficients of fluid φ to another. The C_d depends on the properties of DPE (as a rigid or spherical etc) and usually determined empirically from experiment data. In this study, C_d is estimated by [38],

$$C_d = \frac{24}{Re}(1 + 0.15Re^{0.687}) \tag{7}$$

The force of buoyancy (the body force, $F_{b,\varphi}$) is implemented to the pressure gradient, as suggested by Rusche to get the pressure modified [39], as such that the hydrostatic pressure is subtracted from the static pressure which is more convenient for treatments of the contact of each phase with wall.

In the sediments or porous zones, the macro-scale resistance forces for each phase φ as the fluid-solid interaction force can be predicted by [40]

$$\bar{M}_{\varphi,s} = \left(\frac{\mu_{\varphi}}{K k_{r\varphi}}\right)\bar{U}_{\varphi} \tag{8}$$

where μ is viscosity of fluids, the intrinsic permeability K (m^2) has been set as discussed in section 2, and $k_{r\varphi}$ the relative permeability. The correlation of relative permeability proposed by Brooks and Corey [41], which is an extended version of Corey's proposal [42], is applied in this study,

$$k_{r\varphi} = \begin{cases} (S_e)^{\frac{2+3\lambda}{\lambda}} & \varphi = 0 \\ (1 - S_e)^2\left(1 - S_e^{\frac{2+3\lambda}{\lambda}}\right) & \varphi = 1 \end{cases} \tag{9}$$

where, S_e is the effective saturation and defined as:

$$S_e = \frac{S_w - S_{wr}}{1 - S_{wr}} \tag{10}$$

with S_w as the wetting phase (brine) saturation and S_{wr} the residual saturation of the wetting phase (brine). λ is a parameter for distribution of pore sizes, which is set to $\lambda > 2$ for narrow distributions and $\lambda \leq 2$ for wide distributions [41].

The mass conservation of each component in a considered element, can be derived as,

$$\frac{\partial \varepsilon \alpha_\varphi \rho_\varphi Y_{\varphi,k}}{\partial t} + \frac{\partial \varepsilon \alpha_\varphi \rho_\varphi Y_{\varphi,k} \overline{U}_{\varphi,j}}{\partial x_j} - \frac{\partial \varepsilon \alpha_\varphi D_{\varphi,k} \nabla Y_{\varphi,k}}{\partial x_j} = \dot{S}_{\varphi,k} \tag{11}$$

where Y_φ is the mass fraction of the species, $Sc_\varphi = 0.7$ is the Schmidt number for prediction of effective diffusivity, and $\dot{S}_{\varphi,k}$ denotes the mass transfer rate of species. In this study, only the CO_2 solution, $Y_{1,1}$ in brine and seawater is considered, for which, the $\dot{S}_{1,1}$ is the dissolution rate of CO_2,

$$\dot{S}_{m,\varphi} = k_{\varphi,k} A_{\varphi,k} (C_s - C_o) \tag{12}$$

where C_s is the solubility (in condensation) of CO_2 gas and C_o is the background concentration of dissolved CO_2 in brine/seawater; $k_{\varphi,k}$ is the effective mass transfer coefficient and $A_{\varphi,k}$ is the effective interfacial area between fluids, which are predicted by adjustments with the data from experiments [43] [44] .

3 Simulations of STEMM-CCS experiments

The AnsdMF model is applied to investigate the dynamics of plume developments of CO_2 gas and CO_2 solution in sediments for STEMM-CCS field experiments. The simulations consist of two parts, the

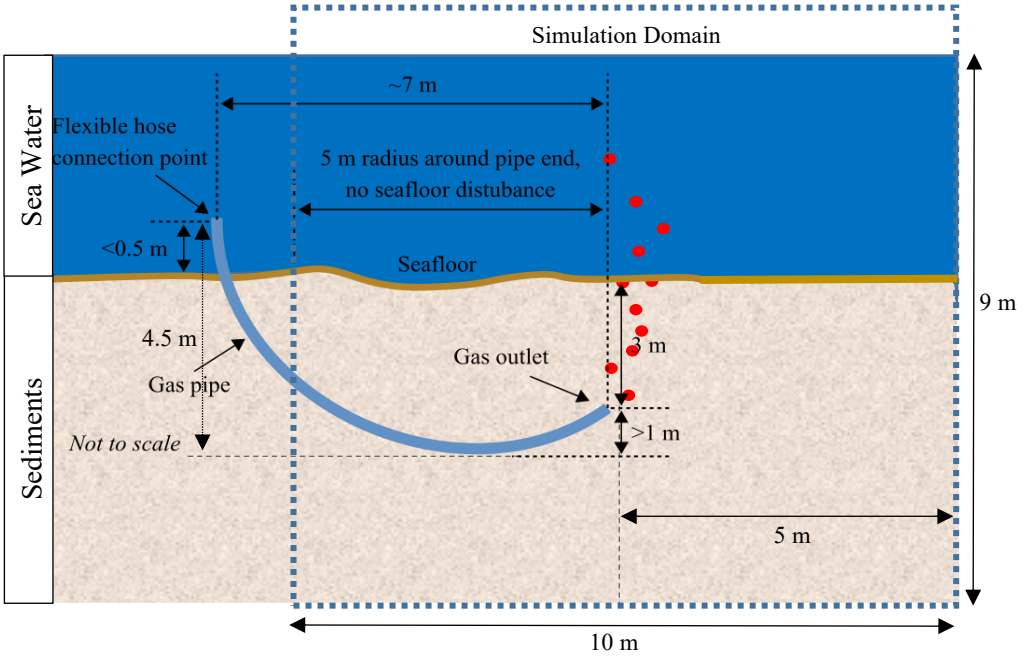

***Figure 5**. The schematics of model simulation set up and computation domain for simulations of STEMM-CCS field experiment*

pre-experiment simulations of CO_2 injection through injection pipe and the simulations of CO_2 dispersion through sediments with variant structures. The schematics of the computation domain and the related scales are shown in Fig. 5 for reference.

3.1 Pre-Experiment Simulation of CO_2 injection test

The flows of CO_2 through customized design of gas release system for STEMM-CCS experiment are simulated to predict the interactions of injected CO_2 gas with pre-loaded water in the U-shaped injection pipe, the dimensions and arrangement of the injection system can refer to Fig. 5. The intention of this simulation is to exam the possibility of back flow due to overburden sediments under a pressure of 12 bar and gas–liquid two-phase stratified flow behaviour at bottom curvature of pipe, which are the most concerns for the design of CO_2 injection system.

Results from model simulations identify the separations of injected CO_2 in the injection pipe at lower injection rate of 5.7 Kg/day, or at the initial stage of the injection. The dynamics of injected gas and water interactions at injection time of 3.5 minutes are discussed as follows. As for the downward part of the pipe (the left part of pipe shown in Fig. 6 (a)), the gas can manage to 'push' the water moving forward, while a separation of gas from water occurs closing to stationary point (Fig. 6, a and d).

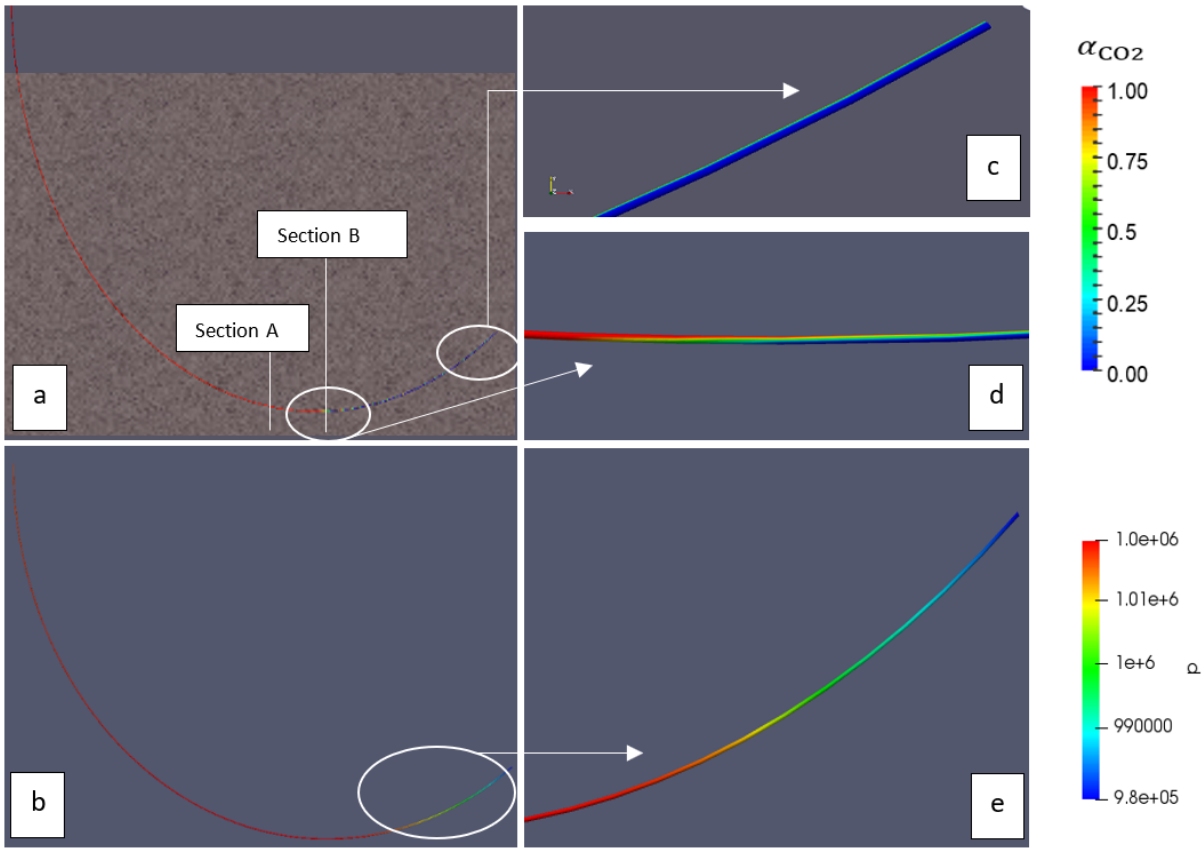

Figure 6: *Model simulation results: (a)* CO_2 *(Red) distribution in injection pipe at injection rate of 5.7 Kg/day into water (Blue) pre-loaded in the pipe; (b) Pressure distribution in the pipe; (c) volume fraction* (α_{CO_2}) *at the outlet shows* CO_2 *gas flows through only partial of the pipe section; (d) the CO2 volume fraction around bottom curvature; and (e) Pressure distribution zoom-in the outlet section of the pipe.*

This separation may be due to the interactions of inertia of water and the buoyancy of the gas [45, 46]. As such, in the upward part of the pipe, only partial of gas CO_2 can flow upwards and towards further (or inject) into the sediments, as shown in Fig. 6c & 6d.

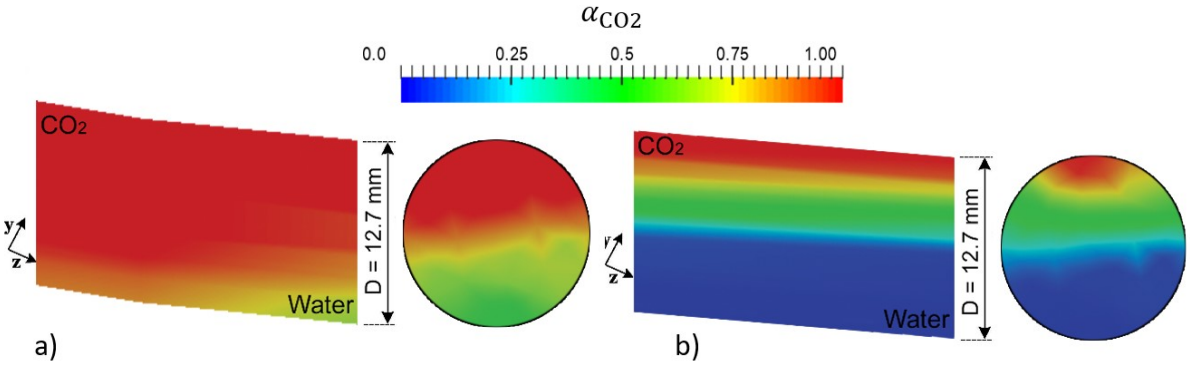

Figure 7. *Interactions of gas CO_2 ($\alpha_{CO_2} = 1$), CO_2 solution ($0 < \alpha_{CO_2} < 1$) and water ($\alpha_{CO_2} = 0$) in pipe at different sections indicated by CO_2 volume fraction, α_{CO_2}, from model simulations. a) a wave-like interface between CO_2 gas and CO_2 solution in the pipe at section A closing to the arc as indicated in Fig. 6 (a); b) the stratifications of gas CO_2, CO_2 solution and water in pipe closing to the centre of arc at section B shown in Fig. 6 (a).*

A wave-like interface between CO_2 and water indicated by CO_2 volume fraction shows the instability of the flow by interactions of CO_2 and water (Fig.7, a). The unstable stratification is identified at the interface between CO_2 solution and water, as shown at the arc of the pipe in Fig. 7, b).

Because of the separation, model simulations suggest that a higher injection pressure should be provided in order to keep the CO_2 gas injection rate, which is identified by the data from field experiment during the initial stage of injection [31].

3.2 Investigation on the plume developments of CO_2 gas and CO_2 solution through sediments to water column

The model is then set for STEMM-CCS field experiments to diagnose of dynamics of CO_2 plume developments in sediments to ocean bottom boundary layer. The diagnostics are performed by injecting CO_2 into the reconstructed sediments with variants of cut-off grain size (refer to section 2.2) in comparisons with field observation data, the time of CO_2 breakthrough. The three-dimensional 10m x 9m x 5m computation domain is set with non-uniform mesh includes a 6.0 m thick heterogeneous layer of sediments and a 3 m ocean on top of sediments as shown in Fig. 4 (b) and Fig.5. The ocean current data from field observation is used to set the flows of water on the top of sediments.

The results of diagnostic simulations of the CO_2 plume developments through sediments reconstructed by setting the cut-off particles sizes from 30 μm to 60 μm are listed in Table 1 for cases I to VIII. An injection rate of 6 Kg/day CO_2 is used for the diagnostic discussions. The parameters for case checking are the CO_2 eruption time, the size of the CO_2 gas plume at ocean floor, the percentages of dissolved

CO_2 in the sediments and those leaked to the ocean at the time of CO_2 eruption. The mesh independent test was performed to exclude the effects from grid-setting. The minimum mesh size is 0.5mm setting at regions closing to the injection port.

The first case is for the sediments using the original data shown in Fig 3, for which the cut-off particle size is zero. This means that the original sediment filled with clay or sands is kept without fractures or pockmarks. The simulation results show that the injected CO_2 gas takes about 2.5 hours to flow through the sediment at a dispersion rate of 1.2 m/hr. Obviously, it is not the case of the field experiment, for which the pockmarks were observed and eruption time is about 16 min [31].

When setting the cut-off particles, as listed in Table, I, the numerical experiment tests predicted that the larger the cut-off particle size sets, the shorter the eruption time is, which decreases nonlinearly at a rate of 10 min per cut-off particle size. The same trend is for the area of CO_2 gas plume at sediment surface (D_E), which linearly decreases at a rate of 0.05 m per cut-off particle size. It seems not too sensitive to the dissolution of CO_2, which varies from 29% to 26% of the total injected CO_2 with time periods from 108 to 16 minutes. It is also noticed that the eruption time is approaching to the time observed from field experiment, when the cut-off size up to 60 μm. At the point of model diagnostics, this means that the sediments in the field experiments should form some pockmarks and create some fracture or 'channels' by CO_2 gas injection and dispersions to push and move the fine size grains/particles (< cut-off size) flowing upward.

This can be partially demonstrated by the plumes, as shown in Fig.8 (note, the bottom part is sediments and top part is ocean), developed in variant of sediments at the eruption time. No significant differences are observed in general structure of the plumes from cut-off grain size < 40 μm, for which three horizontal branches are formed. The same for those of cut-off grain size at 40 μm to 50 μm, where only one horizontal branch forms. The CO_2 can manage to flow through the pathway with larger porosities, which are the left-side of the plumes for sediments of a-d, as shown in Fig. 8 with the red colour. When the cut-off grain size is set up to 50 μm to 60 μm, the plume could only develop within a certain horizontal region, meanwhile, two vertical flow pathways/channels (the red colour in Fig 8, f-h) are created to allow CO_2 gas to disperse fast toward to sediment surface without much dispersion horizontally. It is interesting to see a cap-like plume at the top layer of the sediments for all of the cases, which are the results of effecting from the ocean current and the relative larger porosities.

Table 1: *results for various reconstructed model at grain size cut-off along with dissolution and plume diamter at the time of eruption/leakage*

Case	Cut-off Particle Size limit ($D_{p)}$ (μm)	Eruption Time (T_E) (minutes)	CO_2 Plume Size on the seafloor at Eruption (D_E) (m)	M_{dis}/M_{total}	Permeability (K) (m^2)
a	30	108	3.40	0.290	4.40952×10^{-14}
b	36	72	3.21	0.289	9.83845×10^{-13}
c	40	64	2.98	0.284	1.01031×10^{-13}
d	45	42	2.66	0.277	1.14303×10^{-12}
e	50	36	2.38	0.274	1.64711×10^{-12}
f	52	33	2.31	0.270	2.67462×10^{-12}
g	55	26	2.16	0.269	3.53409×10^{-12}
h	60	16	2.08	0.267	8.32981×10^{-12}

From the numerical diagnoses, the sediments with cut-off grain size of 60 μm is considered for the simulations of the STEMM-CCS field experiments to be discussed in the next section.

3.3 Simulations of CO_2 plume developments of STEMM-CCS field experiment

The developed model, AnsdMF, is applied to simulate the processes of CO_2 plume development in field experiment by injection of CO_2 at the rates recorded from experiments into the reconstructed sediments, which is diagnosed in last section with cut-off particle size of 60 μm. The CO_2 gas plume developed with time through sediments to water column is illustrated in Fig. 9 for the period of first 72 hours. It must be noticed that the dissolution of CO_2 in ocean water column is not modelled in the current version of AnsdMF, which means the plume in the water part are those of CO_2 gas bubbles with no dissolution, only for demonstration. However, this may have a neglectable effect on CO_2 gas developments inside the sediments, as no significant peeling down CO_2 solution plume developed from such a small leakage rate [14], therefore, the ocean current dominates the flows of the seawater.

In addition to the vertical dispersion through the pathways that are created during initial development period, it is interesting to see horizontal dispersions of CO_2 in the sediments eventually to form a multilayer plume from injection port. This structure of the plume is dominantly generated by the structure of sediments, the distribution of grain size and porosities. If the dynamic response of sediments on CO_2 dispersion could be modelled, this coupling model would provide the details of interactions among CO_2, brine, the sands of the sediments to predict the formations of chimney, fractures, and pockmarks and the movements of the leakage position on surface of the sediments.

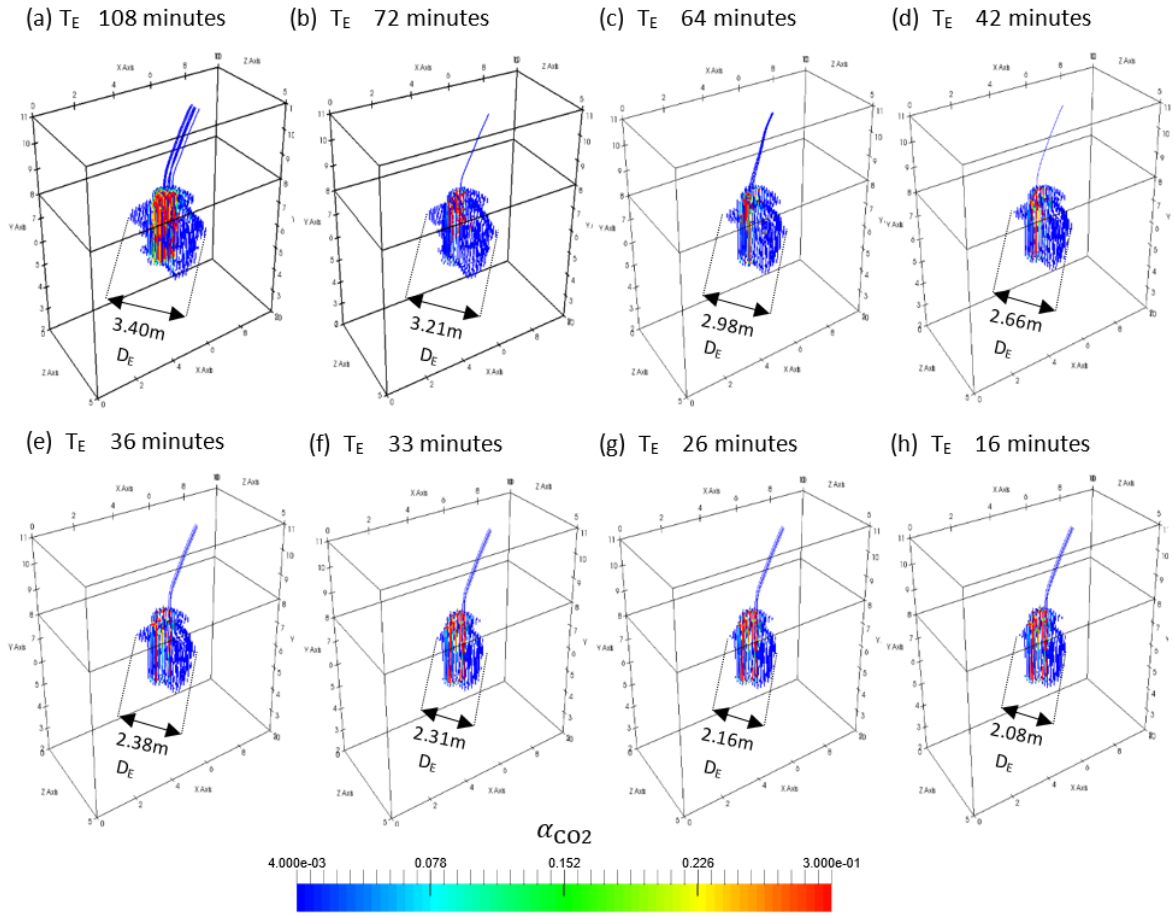

Figure 8: *The plumes of undissolved* CO_2 *in the sediments and water column at the time of breakthrough the sediments with the structure of cut-off grain sizes from 30 to 60 µm. The* D_E *is the maximum diameter of the plume in the sediment.*

The simulations predict that about 98% of injected CO_2 leaks into water column, while, about 1% dissolves into the brine and 1% remains as the gas in the sediment at release time up to 25 hrs. The details on CO_2 plume size in the sediments, the leakage rate, and the ratios of of dissolved CO_2 and gas phase CO_2 in sediments are summarised and listed in Table 2 for th period of field release experiments to the day 11. The CO_2 gas plume developments are as shown in Fig. 9 and Fig. 10. Within the initial period, the CO_2 plume developments, measured by horizontal dispersion, at a rate of 3.75m/day. The

percentage of CO_2 dissolution decreases from 3.8% to 0.2% as the lack of the fresh brine to entrance into the plume.

Table 2: *Summaries of modelling simulation results on plume developments measured by maximum plume diameter, leakage rate, the ratios of dissolved CO_2 (M_{dis}), undissolved CO_2 (M_{undis}) and leaked CO_2 (M_{leaked}) to total injected CO_2 (M_{total}) at experimental date-time*

Time (Hours)	**Day since Injection Started (Day +0)**	**Gas Injection Rate (Kg/Day)**	**Max. Plume Diameter inside Sediment (D_E) (m)**	**Leakage Rate (Kg/Day) (Avg.)**	**M_{dis}/M_{total}**	**M_{undis}/M_{total}**	**M_{Leaked}/M_{total}**
14/05/2019 15:15	*Day +3*	*5.7*	3.51	5.11	0.038	0.024	0.938
15/05/2019 06:47	*Day +4*	*14*	4.72	10.10	0.010	0.008	0.982
17/05/2019 16:53	*Day +6*	*29*	4.92	24.37	0.005	0.006	0.989
19/05/2019 15:49	*Day +8*	*86*	5.11	70.12	0.001	0.001	0.998
22/05/2019 11:15	*Day +11*	*143*	6.51	132.2	0.002	0.001	0.997

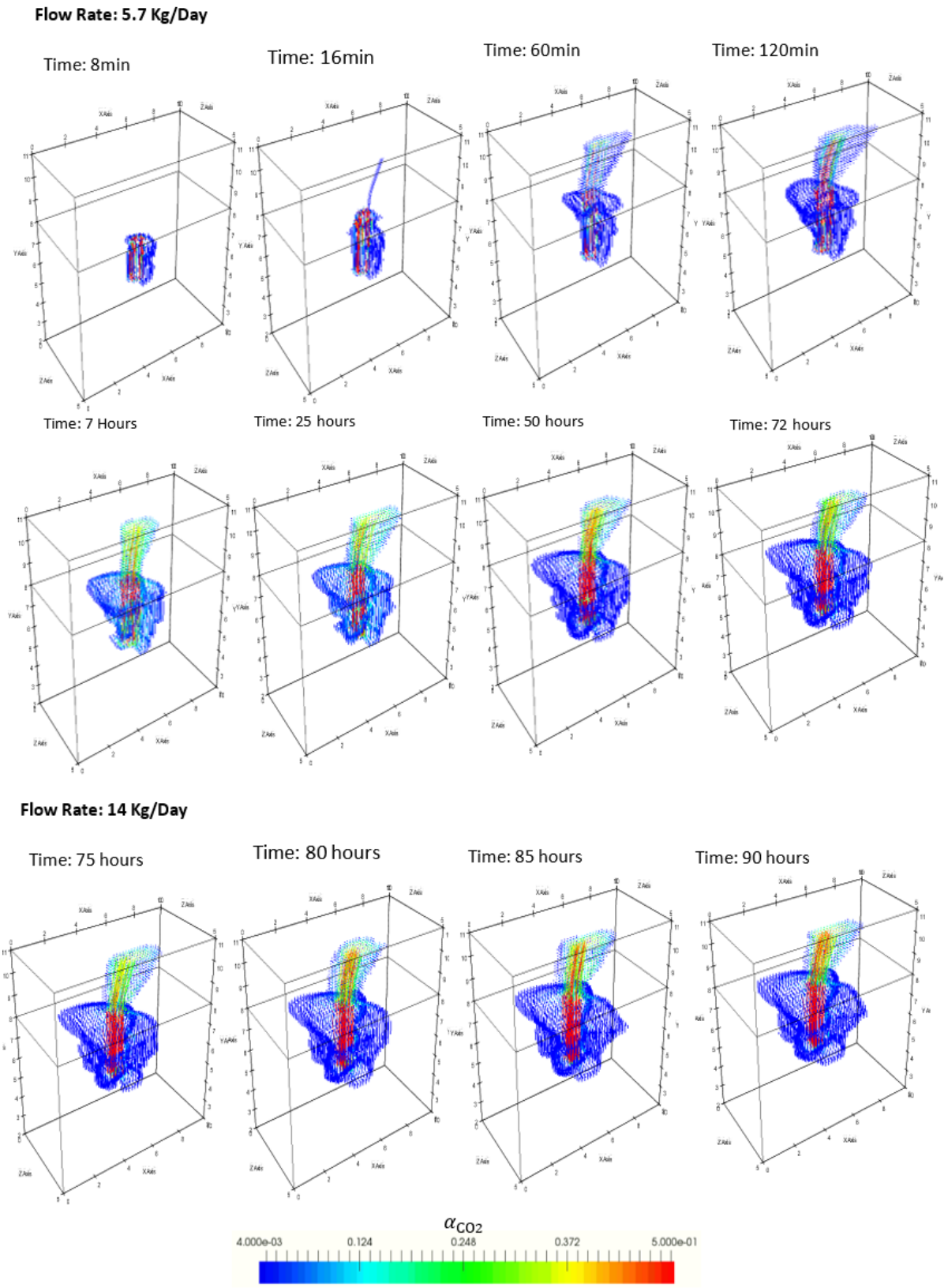

Figure 9: *The model results of developments of CO_2 gas plume in the field experiment up to time of 90 hours.*

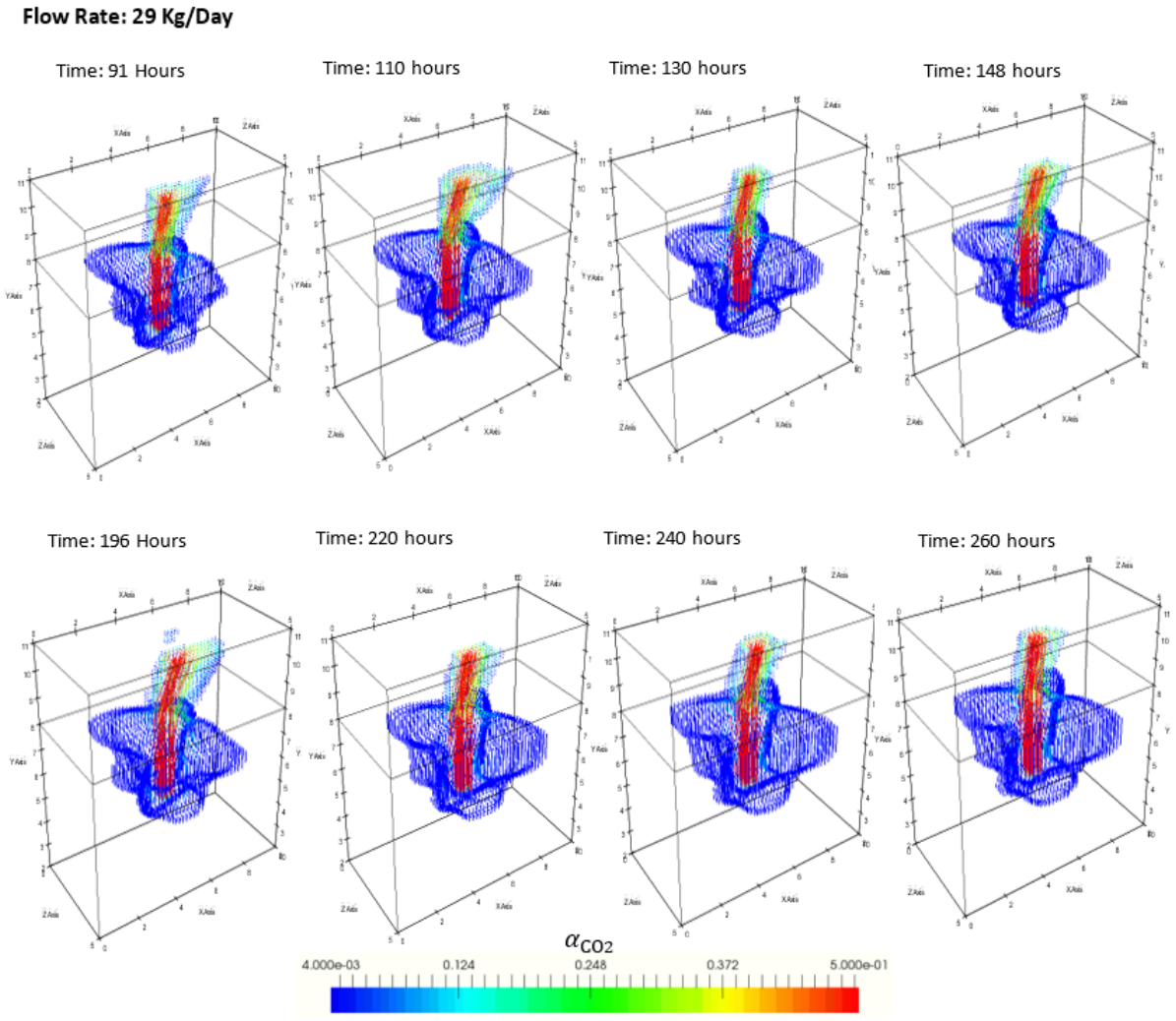

Figure 10: *The model results of developments of CO_2 gas plume in the field experiment up to time of 260 hours.*

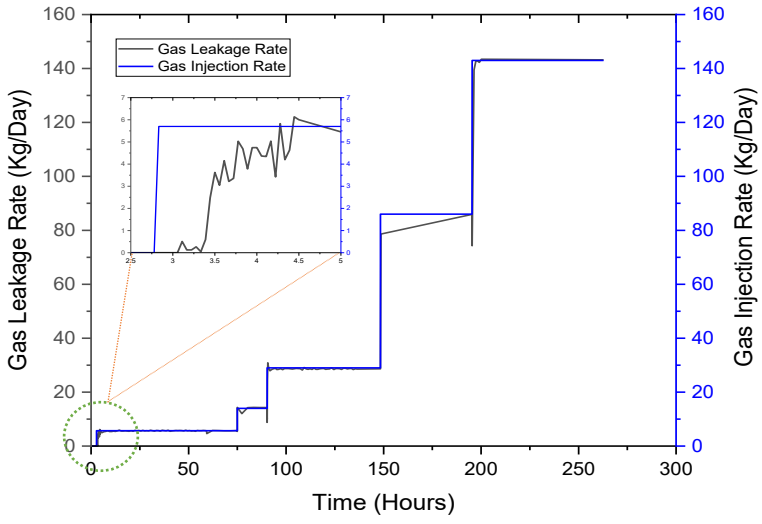

Figure 11: *CO_2 Gas leaking rate from sediments into water column and CO2 injection rate. The sub-Fig show the details withing first 5 days.*

3.3.1 Discussions on CO_2 leakages

To further check the leakage rate, one of the key parameters for the oceanic impacts, the data up to the day 11 of injection from simulations is plotted in Fig. 11 together with CO_2 injection rate. The leakage rates at initial periods of 5 hours are given in an inside figure, which shows that the average leakage rate is about 3.0 kg/day. For comparisons, the observation data and modelling results on leakage rate associating with the injection rate are listed in Table 3 and shown in Fig. 12.

During the release experiment, the CO_2 leakage rate was observed and determined from the eddy pH sensor and the complete procedure of leakage observation is introduce in [47]. According to the discussions [47], an overall CO_2 leakage of 83% ± 14% was estimated under all gas release rates except one of 14.3 kg/day. The details on the field observations on CO_2 leakage rate can be found from publications [47, 48].

Table 3: *Leakage rate data from experiment and simulation*

Injection rate (kg/day)	Leakage rate (Experimental) (kg/day) ±14%	Leakage rate (Simulation) (kg/day)
5.7	2.21	5.11
14.3	1.44*	10.10
28.5	19.8	24.37
85.5	68.7	70.12
143	121.8	132.2

*: The 1.44 kg/day leakage rate at 14.3 kg/day is the weakest observation [47].

The experimental observation data show that the gas leakage initiated from ~2.21 kg/day to ~121.8 kg/day at gas release rate from 5.7 kg/day to 143 kg/day, while, the results from simulations are 5.11 kg/day to 132.2kg/day. As shown in Fig. 12, in general, it can be seen that the model works well in the overall period of injection for the predictions of leakage rates. It has to be noted that it is difficult at the moment to analysis or identify what may result in the differences between model results and observations as both has some uncertainties, e.g., the insufficient in dissolution rate modelling in the modelling side; the possibilities in some undetectable or undetected measurements in the field experiments. If the uncertainties from modelling and observations were considered, the results obtained from model seem acceptable for impact/risk estimation, at least the results from observation and modelling are at the same order of magnitude, especially those of 70.12 kg/day and 68.7kg/day from modelling and observation at the injection rate of 85.5 kg/day.

From modelling simulations, it is identified that initially, the lower CO_2 leakage rate is due to high dissolution rate with sufficient fresh brine for dissolution of CO_2 as the plume developments. The leakage rate increases to 10.10 kg/day due to slowly horizontal dispersion of injected CO_2 and the straightforwardly moving up through the pathway that created from plume initiation, refer to Fig. 9 after

the 75 hours of injection. This mechanism also can explain the larger leakage rate at day 11, which is 121.8 kg/day from observation [47]and143 kg/day from simulation.

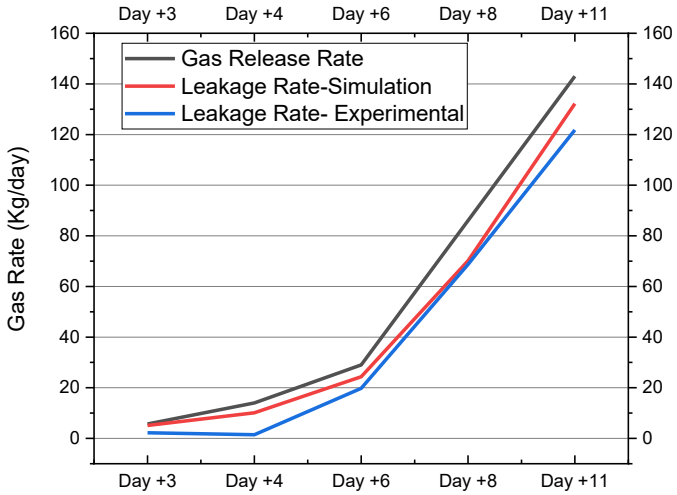

Figure 12: Gas leakage rate comparison with experimental results

These results can be improved by increasing the porosity and grain size resolution. In this study, 2.0cm resolution for porosity and grain sample is used. The increase in number of cores sampling may lead to more accurate sediments structure that can include the precise fracture openings directions, thickness, and locations.

3.3.2 Dissolution of CO_2 in Pore-water

In this section, analysis is focused on CO_2 dissolution in sediment from modelling simulations. The data collected from simulations are the total dissolved CO_2 and remained gas CO_2 in sediment, which are plotted in Fig. 13(a). In order to reveal variations of dissolution with CO_2 injection, the rate of CO_2 dissolution is examined and the data are given in Fig. 13(b). All of the data are collected from plumes of CO_2 solutions, which are shown in Fig. 14 to day 6 and in Fig. 15 for the following days to day 11. From Fig. 13, it can be seen that, as mentioned in the previous section, the injected CO_2 could find unsaturated brine to dissolve during the early period of plume initiations under the lower injections rate. These two factors, lower injection rate and the horizontal dispersions at a rate of 1.17 m/day, refer to the Table 2, leads the maximum dissolution rate, see the first peak in Fig. 13 b), and amount of dissolved CO_2 is relatively larger than those of gas CO_2.

Due to the increases in injection rate to 14kg/day at 75 hrs and 29kg/day at 90 hrs after injection, it turns more gas CO_2 in the sediment than those of dissolved. The increase in injection rate also leads to an increase in dissolution rat, the two peaks shown in Fig. 13 b, at associated times. However, the limitation in the horizontal developments of the plume makes it unable to keep the large dissolution rate, actually, as shown in Fig. 13 b) the average dissolution rate is about 3.0kg/day, which is much smaller than the injection rates. The peaks in dissolution rate are all at the time following the increase in injection rate,

for which, as discussed previously, can be explained by the facts of increase in injection rate leads to the horizontal expansion in CO_2 plume to provide some fresh brine to dissolve CO_2. Once the plume develops to a steady state after each injection increase, the dissolution is then back to the state governed

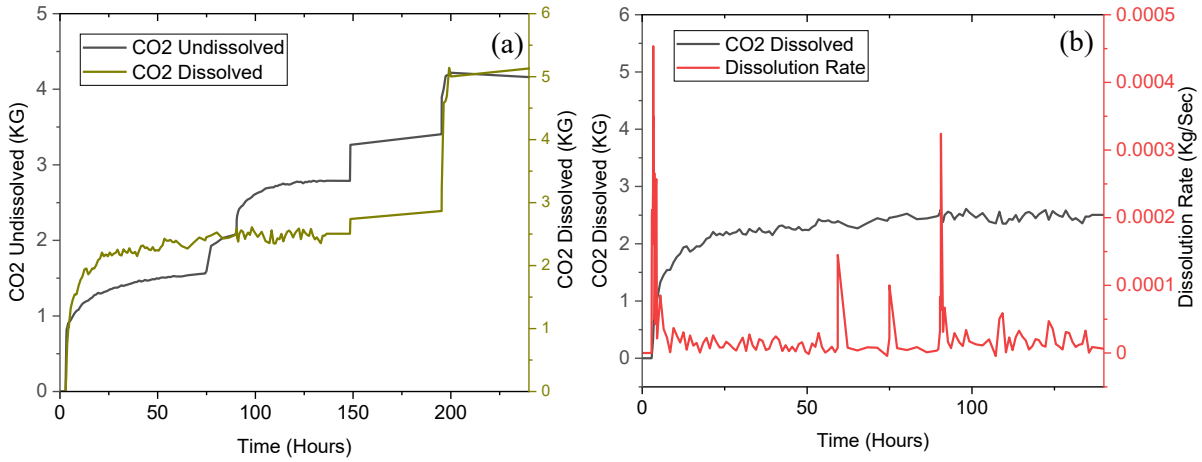

Figure 13: *(a) Total dissolved/undissolved CO_2 in the sediments up to 11 days of CO_2 injection (b) Results showing the total amount of gas dissolved in sediments and dissolution rate*

by the horizontal dispersions of gas CO_2 and a general dissolution rate, as shown in Fig. 13 (b).

The transportation of CO_2 solution vertically and horizontally is slower than that of CO_2 gas driven by buoyancy. This can be seen from CO_2 solution plume development, shown in Fig. 14 and 15. At the centre of the plume, the CO_2 solution reaches to the saturation state (red colour) quickly and develops

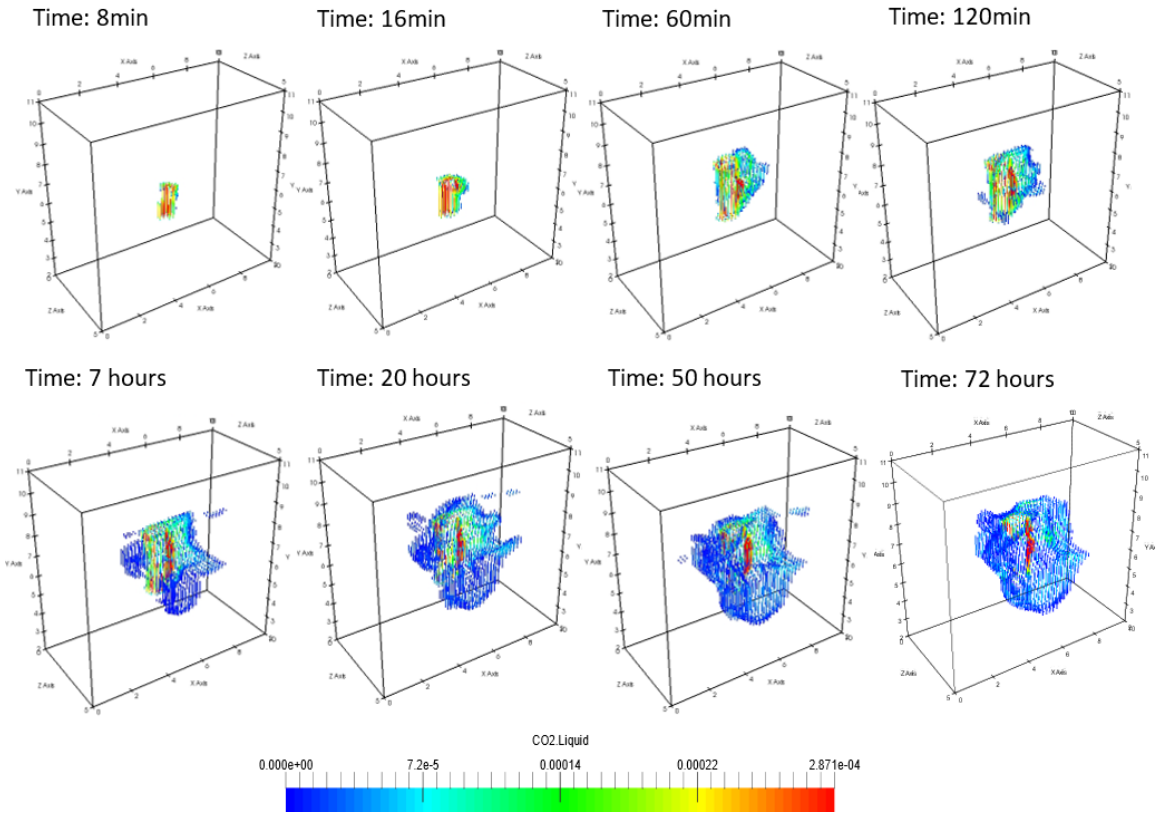

Figure 14: *Time evolutions of dissolved CO_2 plume from initiation to the injection day 3. The plume is demonstrated by CO_2 concentration in CO_2 solution.*

into two branches. The horizontal movement of the plume may be driven by the in-sediment current developed by the ocean current towards to the right side of the computation domain. An obvious sinking

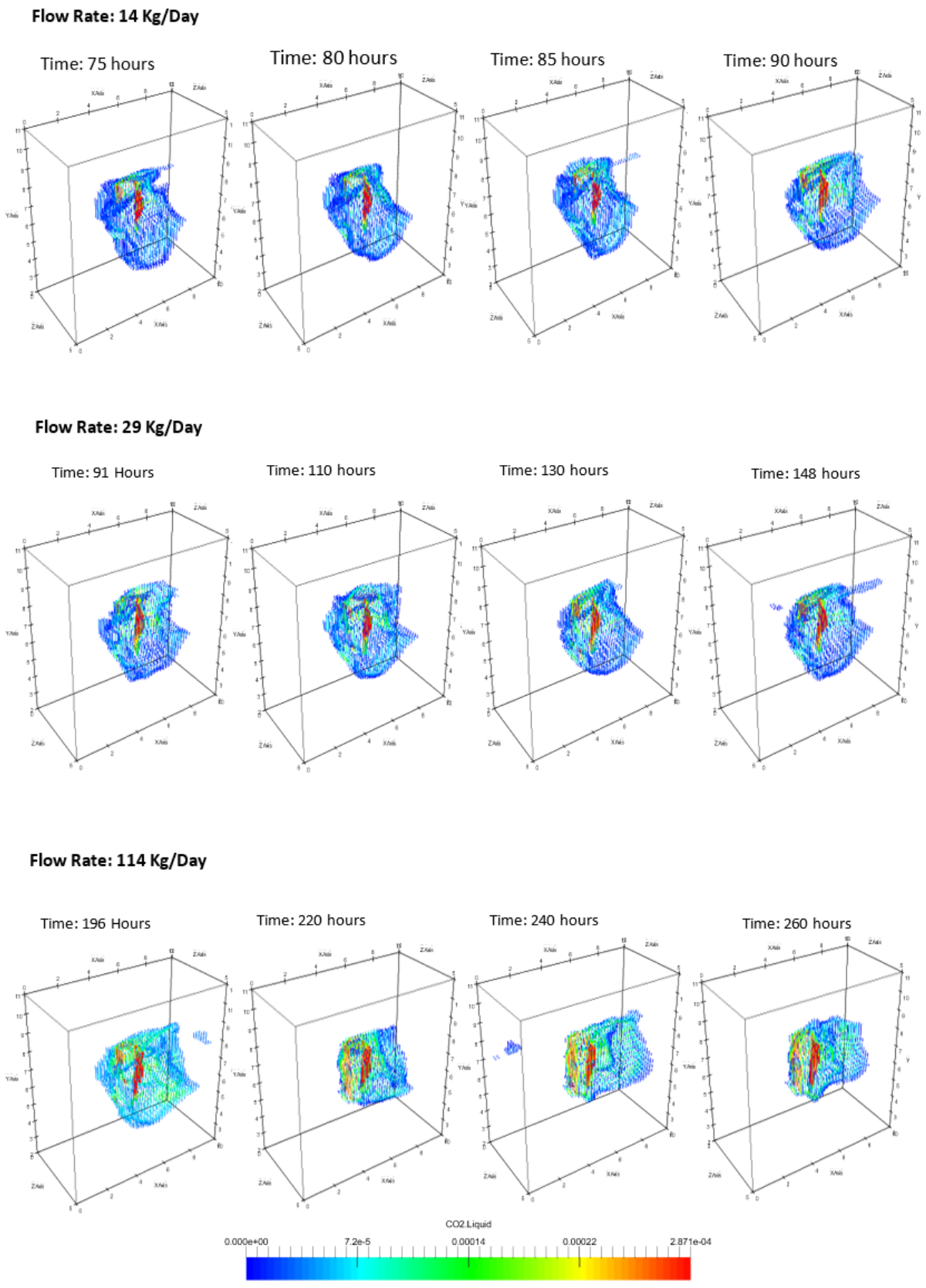

Figure 15: *The model results of developments of CO_2 solution plume in the field experiment from day 3 up to day 11. The plume is demonstrated by CO_2 concentration in solution.*

The distributions of CO_2 as the gas phase and solution in sediment and those leaked into ocean are given in Fig. 16, from which it is clearly seen that up to 10 hours of injection, about 90% of injected CO_2 are leaked into the ocean water column from sediments in this field experiments.

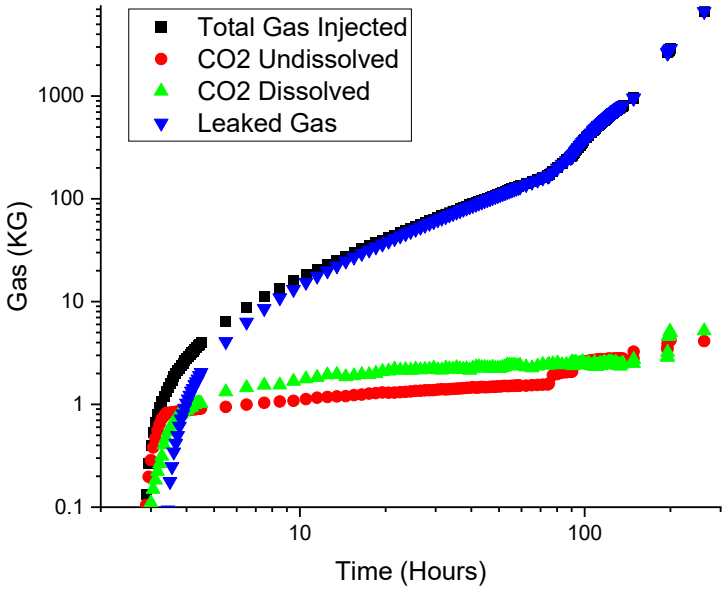

Figure 16: *The modelled distribution of injected CO_2, dissolved and undissolved CO_2 in sediments, and CO_2 leaked to water column*

3.3.3 Ocean tide impact on dissolution and leakage rate

In order to find the tide (pressure) effect on the CO_2 dissolution rate and leakage, sinusoidal pressure wave was set on top of domain to simulate the physical behaviour of ocean tide as shown in Fig. 17. No significant effect is observed.

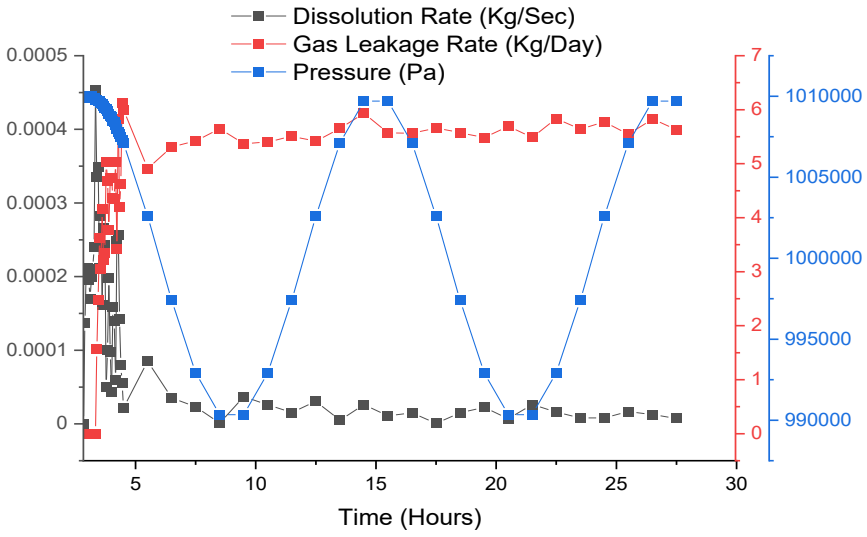

Figure 17*: Effect of tilde (pressure) on dissolution rate and leakage rate*

It looks that the fluctuations of dissolution rate somehow are conceited with the fluctuations of ocean current, as shown in Fig. 18, while are more dementated by injection rate.

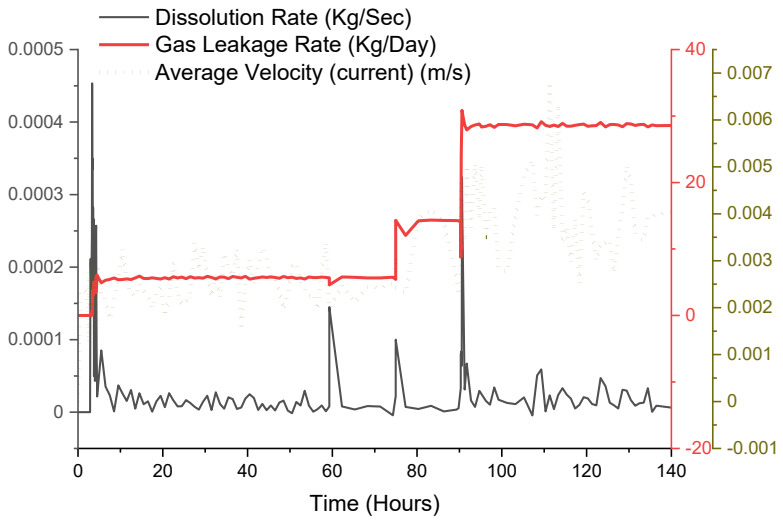

***Figure 18**: Effect of ocean current on dissolution rate and leakage flux*

4 Conclusion

The developed "An arbitrary Navier-Stokes-Darcy multi-fluid flow model" (AnsdMF) is applied to simulate a controlled CO_2 release experiment in order to diagnosis the mechanisms of the evolution of gas in near subsurface migration pathways and breakthrough in the seawater. By simulating the CO_2-Water two phase flow in the complex geoformations based with fractures, channels and pockmark physical data, it is identified that the model is capable of predicting the major mechanisms of CO_2 dispersion and dissolution in the sediments with complex structures of chimney/fracture/pockmarks.

By the reconstructed sediment, diagnosed by CO_2 eruption time, the model predicts for this experiment that the most of CO_2 stored in sediment in solution phase are dissolved within the first day of injection at a peak dissolution rate of 0.35g/sec at the first hour of gas injection. The preliminary results of CO_2 leakage rates and total leaked CO_2 from model simulations are generally agreed with those of field observations. However, the uncertainties from both the developed model and observation measurements suggest the further investigations on the mechanism of CO_2 dissolution in sediments. One of the key conclusions from modeling diagnostic studies is that the structure properties of sediment play the key role on CO_2 leakage, meanwhile, it is suggested that the CO_2 gas be able to manage to create the pathways in sediment by replacing or removing the mad or clay to create the fractures or 'chimney' to flow through. The dynamics and the mechanisms of this fractures or 'chimney' creation should be well investigated and a model should be developed.

5 Acknowledgements

This research is supported by STEMM-CCS project received funding from the European Union's Horizon 2020 research and innovation programme under grant agreement No. 654462. In-kind contributions from the University of Bergen are gratefully acknowledged. The authors also acknowledge the Research Council of Norway through the CLIMIT program funded project no 254711 (Baymode).

References

1. NOAA. Atmospheric CO2, Mauna Loa Observatory. <http://co2now.org/images/stories/data/co2-mlo-monthly-noaa-esrl.pdf> (accessed 03.06.20). 2020.
2. IPCC, Summary for Policymakers. In: Global Warming of 1.5°C. An IPCC Special Report on the impacts of global warming of 1.5°C above pre-industrial levels and related global greenhouse gas emission pathways, in the context of strengthening the global response to the threat of climate change, sustainable development, and efforts to eradicate poverty [Masson-Delmotte, V., P. Zhai, H.-O. Pörtner, D. Roberts, J. Skea, P.R. Shukla, A. Pirani, W. Moufouma-Okia, C. Péan, R. Pidcock, S. Connors, J.B.R. Matthews, Y. Chen, X. Zhou, M.I. Gomis, E. Lonnoy, T. Maycock, M. Tignor, and T. Waterfield (eds.)]. World Meteorological Organization, Geneva, Switzerland, 32 pp. 2018.
3. Freund, P. and W.G. Ormerod, Progress toward storage of carbon dioxide. Energy Conversion and Management, 1997. **38**: p. S199-S204.
4. Han, J.-H., J.-H. Ryu, and I.-B. Lee, A preliminary infrastructure design to use fossil fuels with carbon capture and storage and renewable energy systems. International Journal of Hydrogen Energy, 2012. **37**(22): p. 17321-17335.
5. Oleynik, A., et al., Optimal sensors placement for detecting CO2 discharges from unknown locations on the seafloor. International Journal of Greenhouse Gas Control, 2020. **95**: p. 102951.
6. Feely, R.A., et al., Chemical and biological impacts of ocean acidification along the west coast of North America. Estuarine, Coastal and Shelf Science, 2016. **183**: p. 260-270.
7. Sokołowski, A., D. Brulińska, and E. Sokołowska, Multimarker response of the ragworm Hediste diversicolor (Polychaeta) to seawater acidification derived from potential CO2 leakage from the CCS sub-seabed storage site in the Baltic Sea. Journal of Experimental Marine Biology and Ecology, 2020. **530-531**: p. 151433.
8. Yang, Y.-M., et al., Integration of wellbore pressure measurement and groundwater quality monitoring to enhance detectability of brine and CO2 leakage. International Journal of Greenhouse Gas Control, 2019. **85**: p. 143-155.
9. Amaro, T., et al., Effects of sub-seabed CO2 leakage: Short- and medium-term responses of benthic macrofaunal assemblages. Marine Pollution Bulletin, 2018. **128**: p. 519-526.
10. Jones, D.G., et al., Developments since 2005 in understanding potential environmental impacts of CO2 leakage from geological storage. International Journal of Greenhouse Gas Control, 2015. **40**: p. 350-377.
11. Molari, M., et al., CO2 leakage can cause loss of benthic biodiversity in submarine sands. Marine Environmental Research, 2019. **144**: p. 213-229.
12. Li, C., et al., A new method to protect the cementing sealing integrity of carbon dioxide geological storage well: An experiment and mechanism study. Engineering Fracture Mechanics, 2020. **236**: p. 107213.
13. Uemura, S., et al., Experiment on liquid and supercritical CO2 distribution using micro-focus X-ray CT for estimation of geological storage. Energy Procedia, 2011. **4**: p. 5102-5107.
14. Dewar, M., et al., Small-scale modelling of the physiochemical impacts of CO2 leaked from sub-seabed reservoirs or pipelines within the North Sea and surrounding waters. Marine Pollution Bulletin, 2013. **73**(2): p. 504-515.

15. Caudron, C., A. Mazot, and A. Bernard, Carbon dioxide dynamics in Kelud volcanic lake. Journal of Geophysical Research: Solid Earth, 2012. **117**(B5).
16. McGinnis, D.F., et al., Discovery of a natural CO2 seep in the German North Sea: Implications for shallow dissolved gas and seep detection. Journal of Geophysical Research: Oceans, 2011. **116**(C3).
17. Esposito, A., G. Giordano, and M. Anzidei, The 2002–2003 submarine gas eruption at Panarea volcano (Aeolian Islands, Italy): Volcanology of the seafloor and implications for the hazard scenario. Marine Geology, 2006. **227**(1): p. 119-134.
18. Kim, J., et al., CO2 leakage detection in the near-surface above natural CO2-rich water aquifer using soil gas monitoring. International Journal of Greenhouse Gas Control, 2019. **88**: p. 261-271.
19. Rhino, K., et al., The Demo-CO2 project: Monitoring and comparison of two shallow subsurface CO2 leakage experiments with gas tracer associated in the carbonate vadose zone. International Journal of Greenhouse Gas Control, 2016. **53**: p. 207-221.
20. Drange, H., G. Alendal, and P.M. Haugan, A bottom gravity current model for CO2-enriched seawater. Energy Conversion and Management, 1993. **34**(9): p. 1065-1072.
21. Furre, A.-K., et al., 20 Years of Monitoring CO2-injection at Sleipner. Energy Procedia, 2017. **114**: p. 3916-3926.
22. Rillard, J., et al., The DEMO-CO2 project: A vadose zone CO2 and tracer leakage field experiment. International Journal of Greenhouse Gas Control, 2015. **39**: p. 302-317.
23. Tongwa, P., et al., Evaluation of potential fracture-sealing materials for remediating CO2 leakage pathways during CO2 sequestration. International Journal of Greenhouse Gas Control, 2013. **18**: p. 128-138.
24. Discacciati, M., E. Miglio, and A. Quarteroni, Mathematical and numerical models for coupling surface and groundwater flows. Applied Numerical Mathematics, 2002. **43**(1-2): p. 57-74.
25. Du, G., Y. Hou, and L. Zuo, Local and parallel finite element methods for the mixed Navier–Stokes/Darcy model. International Journal of Computer Mathematics, 2016. **93**(7): p. 1155-1172.
26. Cai, M., M. Mu, and J. Xu, Numerical solution to a mixed Navier-Stokes/Darcy model by the two-grid approach. SIAM Journal on Numerical Analysis, 2009. **47**(5): p. 3325-3338.
27. Chidyagwai, P. and B. Rivière, Numerical modelling of coupled surface and subsurface flow systems. Advances in Water Resources, 2010. **33**(1): p. 92-105.
28. Blackford et al., Blackford, Jerry and Alendal, Guttorm and Artioli, Yuri and Avlesen, Helge and Cazenave, Pierre and Chen, Baixin and Dale, Andy and Dewar, Marius and García-Ibáñez, Maribel I. and Gros, Jonas and Gundersen, Kristian and Haeckel, Matthias and Khajepor, Sorush and Lessin, Gennadi and Oleynik, Anna and Omar, Abdirahman M. and Saleem, Umer, Ensuring Efficient and Robust Offshore Storage – The Role of Marine System Modelling. 14th Greenhouse Gas Control Technologies Conference Melbourne 21-26 October 2018 (GHGT-14) . Available at SSRN: https://ssrn.com/abstract=3365821. 2018.
29. Taylor, P., et al., A novel sub-seabed CO2 release experiment informing monitoring and impact assessment for geological carbon storage. International Journal of Greenhouse Gas Control, 2015. **38**: p. 3-17.
30. Dean, M. and O. Tucker, A risk-based framework for Measurement, Monitoring and Verification (MMV) of the Goldeneye storage complex for the Peterhead CCS project, UK. International Journal of Greenhouse Gas Control, 2017. **61**: p. 1-15.
31. Flohr, A., et al., "Towards improved monitoring of offshore carbon storage: A real-world field experiment detecting a controlled sub-seafloor CO2 release," , no. This Issue. International Journal of Greenhouse Gas Control, 2020.
32. Flohr, A., et al., Towards improved monitoring of offshore carbon storage: A real-world field experiment detecting a controlled sub-seafloor CO2 release. International Journal of Greenhouse Gas Control, 2021. **106**: p. 103237.
33. Lichtschlag, A., et al., Impact of CO2 leakage from sub-seabed carbon dioxide storage on sediment and porewater geochemistry. International Journal of Greenhouse Gas Control 2021(STEMM-CCS).

34. Phillips, E. and J. Merritt, Evidence for multiphase water-escape during rafting of shelly marine sediments at Clava, Inverness-shire, NE Scotland. Quaternary Science Reviews, 2008. **27**(9): p. 988-1011.
35. Henderson, N., J. Brêttas, and W. Sacco, A three-parameter Kozeny–Carman generalized equation for fractal porous media. Chemical Engineering Science, 2010. **65**: p. 4432-4442.
36. openfoam.org. (n.d.). OpenFOAM | Free CFD Software | The OpenFOAM Foundation. [online] Available at: https://openfoam.org/.
37. Radwan, A.E., et al., Pore and fracture pressure modeling using direct and indirect methods in Badri Field, Gulf of Suez, Egypt. Journal of African Earth Sciences, 2019. **156**: p. 133-143.
38. Gor, G.Y., H.A. Stone, and J.H. Prévost, Fracture propagation driven by fluid outflow from a low-permeability aquifer. Transport in Porous Media, 2013. **100**: p. 69-82.
39. Rusche, H., Computational Fluid Dynamics of Dispersed Two-Phase Flows at High Phase Fractions, in Department of Mechanical Engineering. 2002, University of London and Diploma of Imperial College.
40. H. P. G. Darcy. Les Fontaines Publiques de la Ville de Dijon. Victor Dalmont,Paris, 1856.
41. Brooks, R.H.a.C., A.T., Hydraulic Properties of Porous Media. Hydrology Papers, No. 3, Colorado State U., Fort Collins, Colorado. 1964.
42. Corey, A.T., The interrelation between gas and oil relative permeabilities. The Interrelation between Gas and Oil Relative Permeabilities, 1954: p. 38-41.
43. Jiang, L., et al., Mass transfer coefficient measurement during brine flush in a CO2-filled packed bed by X-ray CT scanning. International Journal of Heat and Mass Transfer, 2017. **115**: p. 615-624.
44. Jiang, L., et al., Displacement and Dissolution Characteristics of CO2/Brine System in Unconsolidated Porous Media. Transport in Porous Media, 2018. **122**(3): p. 595-609.
45. Duan, J., et al., Hydro dynamic modeling of stratified smooth two-phase turbulent flow with curved interface through circular pipe. International Journal of Heat and Mass Transfer, 2015. **89**: p. 1034-1043.
46. Chisholm, D., Two-phase flow in bends. International Journal of Multiphase Flow, 1980. **6**(4): p. 363-367.
47. Koopmans, D., et al., Detection and quantification of carbon dioxide gas at the seafloor using pH eddy covariance and measurements of plume advection. International Journal of Greenhouse Gas Control, 2021(STEMM-CCS).
48. Loucaides, A.S.D.K.M.H.M.D.M.A.S.P.R.H.S.M.M.M.S., Quantification of a subsea CO2 release with lab-on-chip sensors measuring benthic gradients. International Journal of Greenhouse Gas Control, 2021(STEMM-CCS).